

Flat and almost flat bands in the quasi-one-dimensional Josephson junction array

Daryna Bukatova and Yaroslav Zolotaryuk

Bogolyubov Institute for Theoretical Physics, National Academy of Sciences of Ukraine, Kyiv 03143, Ukraine

E-mail: daryna.bukatova@gmail.com and yzolo@bitp.kiev.ua (corresponding author)

Abstract. The dispersion law for the linear waves in the quasi-one-dimensional array of inductively coupled Josephson junctions (JJ) is derived. The array has a multiladder structure that consists of the finite number of rows ($N \geq 2$) in Y direction and is infinite in X direction. The spectrum of the linear waves (Josephson plasmons) consists of $2N - 1$ branches. Among these branches there is a N -fold completely flat degenerate one that coincides with the Josephson plasma frequency. The remaining $N - 1$ branches have a standard Josephson plasmon dispersion law typical for 1D JJ arrays. Application of the uniform dc bias on the top of each vertical column of junctions lifts the degeneracy and only one flat branch remains unchanged. The rest of the previously flat branches become weakly dispersive. The parameter range where the flatness of these branches is maximal has been discussed.

PACS numbers: 74.81.Fa, 74.50.+r, 73.20.Mf

Keywords: Weak superconductivity, Josephson junctions, Josephson junction arrays, dispersion, plasmons, flat bands.

Submitted to: *J. Phys. C: Solid State Phys.*

1. Introduction

The concept of flat bands (FB) appears in different fields of modern physics [1]. A FB in a spectrum (either energy or phonon) which is a completely dispersionless band $\nabla_{\mathbf{q}}\omega(\mathbf{q}) = 0$ where $\omega(\mathbf{q})$ is the dispersion law of the respective system. The concept of FBs was introduced at first theoretically for electron states in the two-dimensional dice lattice model [2] and, some years later, for the itinerant electrons in the Hubbard model [3]. It was later extended to magnetic systems [4], Josephson junctions (JJs) [5, 6] and Dirac materials [7, 8]. A remarkable consequence of the absence of dispersion is the existence of localized states without breaking the translational invariance of the lattice. Although the first FB models appeared in the late 1980s, only about 10-15 years ago it became possible to observe FBs in different systems and to construct artificial FB systems. For example, several lattice structures with a FB have been

realized in photonic lattices (such as waveguide arrays) [9] and cold atomic gases in optical lattices [10].

The Josephson transmission lines (JTL) or Josephson junction arrays (JJAs) are examples of artificial superconducting systems that can support FBs. For example, the frustrated JJA with FBs has been studied in [6]. It should be mentioned that JJAs are widely studied for applications in quantum computing, for example, possibility of application of JTLs for quantum states readout was discussed theoretically in [11] and studied experimentally later in [12]. Since there has been active research conducted on propagation of current pulses through JTLs [13], it is important to study their dispersion relations.

Ladders of JJs have been actively investigated due to observation of various nonlinear phenomena such as vortex propagation [14, 15], meandering [16] and, finally, prediction [17] and experimental discovery [18, 19, 20] of discrete breathers [21]. It should be noted that while Josephson vortices can exist in the standard 1D JJA, discrete breathers require at least a simple JJ ladder. In [19, 22] it was shown that the Josephson plasmon spectrum for the anisotropic Josephson junction ladder (JLL) with two horizontal rows has a flat band. It is natural to generalize this ladder into a quasi-one-dimensional ladder-like structure with an arbitrary number of horizontal rows N . We will call it an N -row JJA or a quasi-one-dimensional Josephson junction array (Q1D JJA).

The aim of this work is to find and analyse the plasmon spectrum and the corresponding wave amplitudes of the Q1D JJA with the arbitrary number of rows, and, in particular, to establish whether this spectrum still has a FB for any number of rows as it does for the 2-row case.

This paper is organized as follows. In the next section we present the equations of motion for the Q1D JJA with N rows. In the third section the dispersion law for an arbitrary number of rows is obtained and its main properties are discussed. Outlines and conclusions are given in the last section.

2. Equations of motion

We consider a ladder-like array of JJs that consists of a finite number (N) of rows in Y direction as shown in figure 1. The length of each of the rows in the X direction is supposed to be much greater than N . Since we are interested in the plane waves of the array we may assume it to be infinite. The respective phase of the junction will be denoted as $\phi_{n,k}^{(v,h)}$ where the superscript v or h will denote whether the junction belongs to the row (a horizontal one) or to the bridge (a vertical one). The set of subscripts (n, k) enumerates the junction along the X and Y axis, respectively. The array is uniformly biased by the dc current I_B at each (n, N) th junction and the same current is extracted from the each (n, N) th junction. The equations for the time evolution of the Josephson phases for each of the junctions within the resistively and capacitatively shunted (RCSJ) model [23] are given by the following set of equations

$$\frac{C_{v,h}\hbar}{2e} \frac{d^2}{dt^2} \phi_{n,k}^{(v,h)} + \frac{\hbar}{2eR_{v,h}} \frac{d}{dt} \phi_{n,k}^{(v,h)} + I_c^{(v,h)} \sin \phi_{n,k}^{(v,h)} = I_{n,k}^{(v,h)},$$

$$n \in \mathbb{Z}, v : k = \overline{1, N-1}, h : k = \overline{1, N}. \quad (1)$$

Here $C_{v,h}$ is the capacitance of the vertical or horizontal junction, $R_{v,h}$ is its resistance and $I_c^{(v,h)}$ is its critical current, respectively. Finally, $I_{n,k}^{(v,h)}$ is the current that flows through the (n, k) th junction.

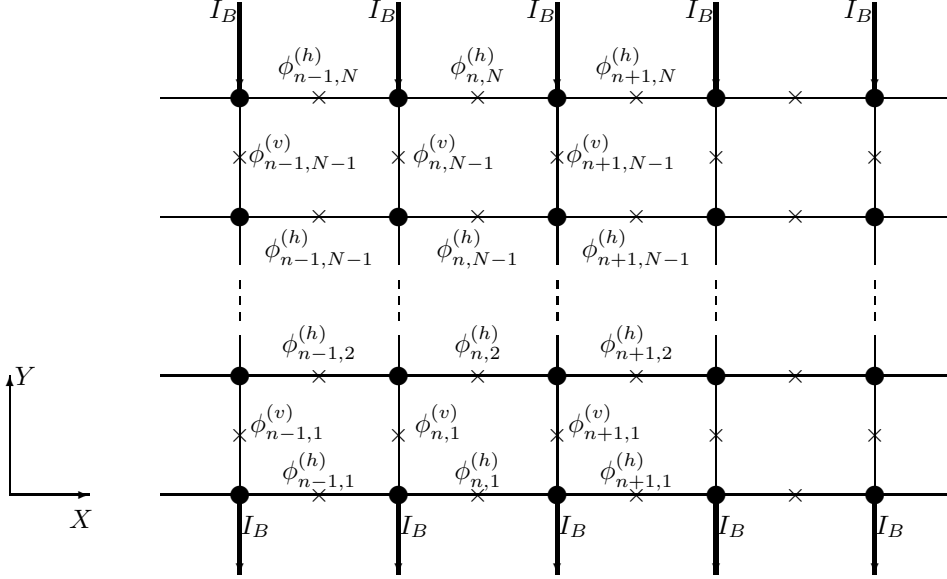


Figure 1: Schematic view of the Q1D JJA with N rows. Only two top and two bottom rows are shown. The crosses \times denote locations of the respective junctions. Thick arrows show the direction and location of the incoming and outgoing dc bias I_B .

For the derivation of the evolution equations one can consult paper [24]. Here only the main points of the derivation will be repeated. For each of these currents we need to write the Kirchoff's equations and the flux quantization law. The latter connects the mesh currents $I_{n,k}^{(m)}$ in the cell formed by the vertical junctions (n, k) and $(n+1, k)$ and horizontal junctions (n, k) and $(n, k+1)$ and the magnetic flux through this cell:

$$I_{n,k}^{(m)} = -\frac{\Phi_{n,k}}{L} = -\frac{\Phi_0}{2\pi L} \left(\phi_{n+1,k}^{(v)} - \phi_{n,k}^{(v)} + \phi_{n,k+1}^{(h)} - \phi_{n,k}^{(h)} \right). \quad (2)$$

Here L is the self-inductance of the cell and $\Phi_0 = \pi\hbar/e$ is the magnetic flux quantum. It is convenient to introduce the dimensionless variables in the following way:

$$\tau = \omega_p t, \quad \gamma = \frac{I_B}{I_c^{(v)}}, \quad \beta_L = \frac{2\pi I_c^{(v)} L}{\Phi_0}, \quad \eta = \frac{I_c^{(h)}}{I_c^{(v)}} = \frac{C_h}{C_v} = \frac{R_v}{R_h}. \quad (3)$$

The coupling constant β_L measures the discreteness of the array. The dimensionless dissipation parameter is then $\alpha = \Phi_0 \omega_p / (2\pi I_c^{(v)} R_v)$, and the time is normalized to the inverse Josephson plasma frequency $\omega_p^{-1} = \sqrt{C_v \Phi_0 / (2\pi I_c^{(v)})}$. Finally, the parameter η measures the anisotropy between the junctions placed in the rows and columns of the array. For the sake of convenience we also introduce the nonlinear operator

$$\mathcal{N}(x) \equiv \ddot{x} + \alpha \dot{x} + \sin x. \quad (4)$$

With the help of this operator the equations of motion are written inside the Q1D JJA

$$\mathcal{N}(\phi_{n,k}^{(v)}) = \gamma + \frac{1}{\beta_L} \left(\hat{\Delta}_x \phi_{n,k}^{(v)} + \hat{\nabla}_x \phi_{n-1,k+1}^{(h)} - \hat{\nabla}_x \phi_{n-1,k}^{(h)} \right),$$

$$n \in \mathbb{Z}, k = \overline{1, N-1}, \quad (5)$$

$$\mathcal{N}(\phi_{n,k}^{(h)}) = \frac{1}{\eta\beta_L} \left(\hat{\Delta}_y \phi_{n,k}^{(h)} + \hat{\nabla}_x \phi_{n,k}^{(v)} - \hat{\nabla}_x \phi_{n,k-1}^{(v)} \right),$$

$$n \in \mathbb{Z}, k = \overline{2, N-1}, \quad (6)$$

and on the border rows ($k = 1, N$)

$$\mathcal{N}(\phi_{n,1}^{(h)}) = \frac{1}{\eta\beta_L} \left(\hat{\nabla}_x \phi_{n,1}^{(v)} + \hat{\nabla}_y \phi_{n,1}^{(h)} \right), n \in \mathbb{Z} \quad (7)$$

$$\mathcal{N}(\phi_{n,N}^{(h)}) = -\frac{1}{\eta\beta_L} \left(\hat{\nabla}_x \phi_{n,N-1}^{(v)} + \hat{\nabla}_y \phi_{n,N-1}^{(h)} \right), n \in \mathbb{Z}. \quad (8)$$

These equations represent a system of $2N - 1$ coupled discrete sine-Gordon equations. Here the difference operators introduced for the sake of simplicity are given by the following expressions:

$$\hat{\Delta}_x \phi_{n,k} \equiv \phi_{n+1,k} - 2\phi_{n,k} + \phi_{n-1,k}, \quad (9)$$

$$\hat{\Delta}_y \phi_{n,k} \equiv \phi_{n,k+1} - 2\phi_{n,k} + \phi_{n,k-1},$$

$$\hat{\nabla}_x \phi_{n,k} \equiv \phi_{n+1,k} - \phi_{n,k}, \quad \hat{\nabla}_y \phi_{n,k} \equiv \phi_{n,k+1} - \phi_{n,k}.$$

In real JJAs the dimensionless dissipation parameter α is rather small, $\alpha \lesssim 0.1$ [25]. Moreover, this parameter provides us with information on how fast the Josephson plasmons decay. Our aim is to compute the plasmon spectrum, and, therefore, α will be neglected throughout the next sections.

3. Plasmon bands and their properties

3.1. Dispersion law derivation

In order to calculate the spectrum of the Josephson plasma waves one has to expand the equations of motion (5)-(8) around the steady state

$$\phi_{n,k}^{(v)} = \arcsin \gamma, k = \overline{1, N-1}; \quad \phi_{n,k}^{(h)} = 0, k = \overline{1, N}, n \in \mathbb{Z}, \quad (10)$$

that corresponds to the spatially uniform superconducting state of the whole array. We will study linear waves that propagate in the X direction. The plane wave ansatz for the small deviations from the steady state

$$\begin{aligned} & \left(\delta\phi_{n,1}^{(v)}, \dots, \delta\phi_{n,N-1}^{(v)}, \delta\phi_{n,1}^{(h)}, \dots, \delta\phi_{n,N}^{(h)} \right)^T = \\ & = \left(A_1^{(v)}, \dots, A_{N-1}^{(v)}, A_1^{(h)}, \dots, A_N^{(h)} \right)^T e^{i(qn + \omega\tau)} + \text{c.c.}, \end{aligned} \quad (11)$$

is substituted into the equations of motion (5-8). The resulting characteristic polynomial is given as a determinant of the respective $2N - 1 \times 2N - 1$ matrix. After some calculations (see Appendix A for details) the characteristic polynomial can be written explicitly and, after some manipulations, factorized as

$$\chi(\omega^2) = \frac{1}{\eta^{N-1}} (\omega^2 - 1) \prod_{n=2}^N [d_0 - \alpha_n d_1], \quad \alpha_n = 1 - 2 \cos \frac{\pi(n-1)}{N}, \quad (12)$$

where

$$d_0(\omega^2) = \eta[\omega_i^2(q) - \omega^2] \left(1 + \frac{1}{\eta\beta_L} - \omega^2 \right) - \frac{2(1 - \cos q)}{\beta_L^2}, \quad (13)$$

$$d_1(\omega^2) = -\frac{1}{\beta_L}[\omega_i^2(q) - \omega^2] + \frac{2(1 - \cos q)}{\beta_L^2}, \quad (14)$$

$$\omega_i^2(q) \equiv \sqrt{1 - \gamma^2} + \frac{2}{\beta_L}(1 - \cos q). \quad (15)$$

From here one concludes that there is one flat band with $\omega^2 = 1$. The expression $\omega_i(q)$ is the dispersion law of the biased standard one-dimensional JJA where only the vertical Josephson junctions (see [26, 27]) are present. The rest of the dispersion curves is derived from the equality $d_0 = \alpha_n d_1$. Thus, the whole set of the $2N - 1$ dispersion branches can be written as

$$\omega_0^2 = 1, \quad (16)$$

$$\omega_{\pm n}^2(q) = \frac{1}{2} \left[1 + \omega_i^2(q) + \frac{1 + \alpha_{n+1}}{\eta\beta_L} \right] \pm \sqrt{\frac{1}{4} \left[\omega_i^2 - \left(1 + \frac{1 + \alpha_{n+1}}{\eta\beta_L} \right) \right]^2 + 2(1 + \alpha_{n+1}) \frac{1 - \cos q}{\eta\beta_L^2}}, \quad (17)$$

$$n = \overline{1, N-1}.$$

The constant α_n is given in equation (12) and of importance are the values for $n = \overline{2, N}$. For $N = 2$ rows there is just one value $\alpha_2 = 1$. For $N = 3$ rows there are two values, $\alpha_2 = 0$, $\alpha_3 = 1$. For larger N the values of α_n will pack the interval $] -1, 3[$ more and more densely.

For example, for the particular case of $N = 3$ rows, the dispersion law consists of 5 branches. All of them are shown in figure 2 for different values of dc bias. The branches are indexed in such a way that the dispersionless branch ω_0 is placed in the middle, the branches with positive subscript lie above the ω_0 branch and the branches with the negative subscript lie below. In the $N = 2$ case the formulae (16-17) repeat the already

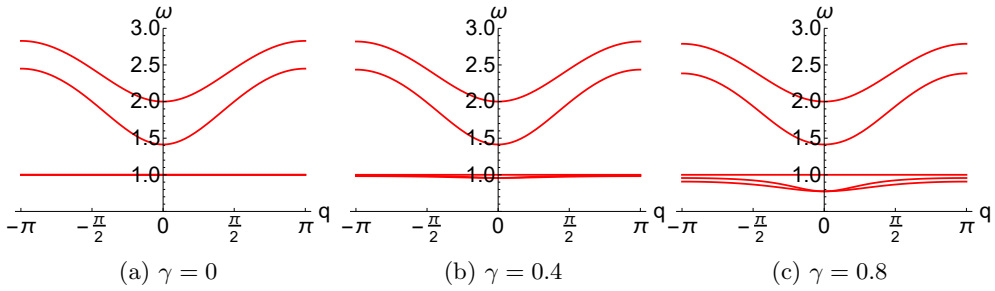


Figure 2: Plasmon bands for $N = 3$ row array, with $\eta = 1$, $\beta_L = 1$ and different values of the dc bias γ .

known result [22]. Thus, generally speaking, the following inequality is valid for all plasmon branches (16)-(17): $\omega_{-N+1} < \dots < \omega_{-1} < \omega_0 = 1 < \omega_1 < \dots < \omega_{N-1}$. The set of branches with $\omega_{n>0}$ appear above the branch $\omega_0 = 1$. They are significantly dispersive and are well separated from each other. The branches $\omega_{n<0}$ depend crucially on the presence of the dc bias. When $\gamma = 0$ they are all *degenerate* $\omega_{-N+1} = \dots = \omega_{-1} = 1$. When the bias is applied the degeneracy is lifted. In that case the branches with $n < 0$ detach from the $\omega_0 = 1$ branch and lie below it. If the bias is small these branches still remain almost flat [see figure 2(b)]. Thus, in the general case of the dc biased Q1D array its plasmon spectrum consists of

- one flat band with $\omega = 1$;
- $N - 1$ strongly dispersive bands;
- $N - 1$ weakly dispersive bands that become completely flat at $\gamma = 0$.

3.2. Dispersion law properties for the different model parameters

In the long wave limit $q \rightarrow 0$ the frequencies of all modes satisfy the following relations:

$$\omega_n(0) = \begin{cases} \sqrt{1 + \frac{1 + \alpha_{n+1}}{\eta\beta_L}}, & n > 0 \\ (1 - \gamma^2)^{1/4}, & n < 0. \end{cases} \quad (18)$$

Thus, even when the degeneracy is lifted at $\gamma \neq 0$ the lower branches remain degenerate at the point $q = 0$ while the upper branches are completely separated. In the limit of strong discreteness ($\beta_L \gg 1$) the difference between the neighboring branches reads $\Delta\omega_n(0) = \omega_{n+1}(0) - \omega_n(0) \approx 2 \sin[\pi/(2N)] \sin[(2n+1)\pi/(2N)](\eta\beta_L)^{-1} + \mathcal{O}[(\eta\beta_L)^{-2}]$.

Next we discuss the properties of the plasmon spectrum as a function of the discreteness parameter β_L . The respective plots for the different values of β_L are given in figures 3a-3c. Naturally, the increase of β_L means larger discreteness effects thus the absolute values of the plasmon frequencies (for modes with $\omega_{n>0}$) increase greatly when β_L decreases [see figure 3a]. In the opposite limit $\beta_L \rightarrow \infty$ the interaction between the cells dies out, hence the dispersion laws that lay above the $\omega_0 = 1$ branch flatten as can be seen in figure 3c. On the other hand, the properties of the lower

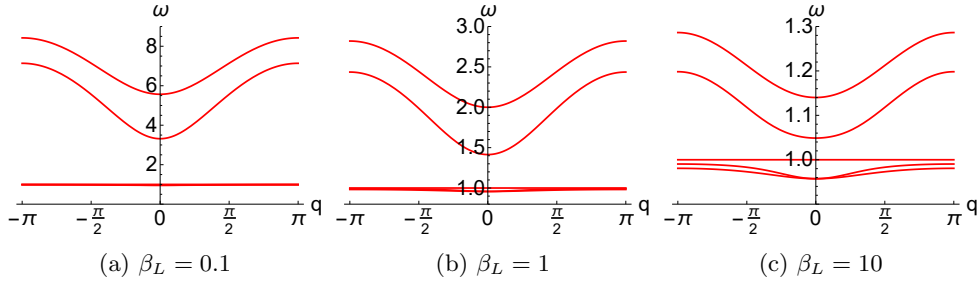


Figure 3: Dispersion relation for the 3-row JJA at fixed values of the dc bias ($\gamma = 0.4$) and anisotropy ($\eta = 1$) and for the different values of the dimensionless inductance β_L .

(almost flat) bands depend mostly on the value of the dc bias as these branches must satisfy $(1 - \gamma^2)^{1/4} \leq \omega_n < 1$ for all $n < 0$.

The role of the anisotropy constant η is demonstrated in figures 4a-4e. This parameter controls the redistribution of the phase oscillations between the horizontal and vertical subsystems. In the limit $\eta \rightarrow 0$ the horizontal oscillations dominate over the vertical ones. First of all, the absolute values of the plasmon frequencies for the branches with $\omega_{n>0} > 1$ increase significantly due to the presence of the $1/\eta$ singularity in the dispersion law. Moreover, the different branches strongly separate from each other (see figure 4a). It is interesting that in the limit of small η and intermediate β_L the dispersive branches (those that lie above $\omega_0 = 1$) have significant gaps between them. The value of the gap between the ω_n and ω_{n+1} branches equals

$$\Delta\omega_n = \omega_{n+1}(0) - \omega_n(\pi) \simeq \sqrt{1 + \frac{1 + \alpha_{n+2}}{\eta\beta_L}} -$$

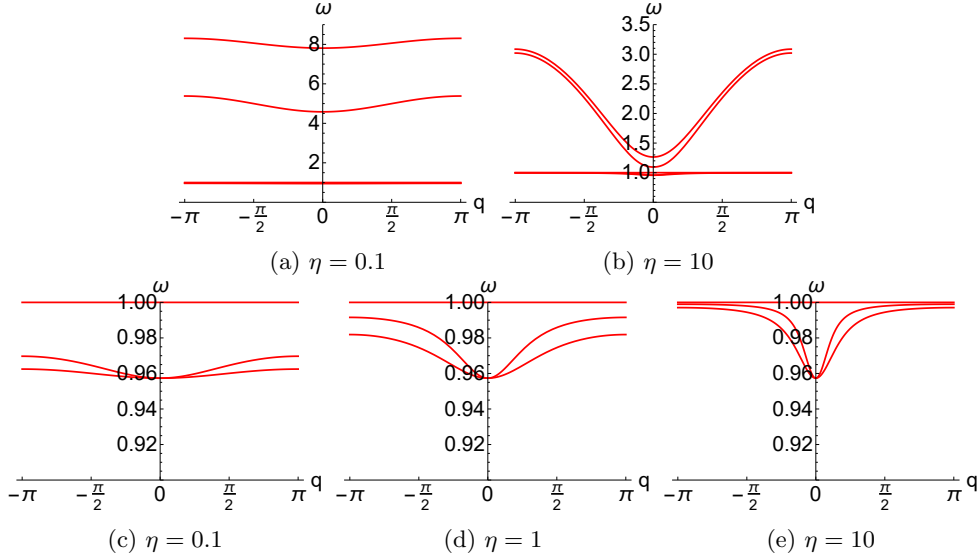


Figure 4: Dispersion relation for the 3-row JJA at the fixed values of the bias and inductance ($\gamma = 0.4, \beta_L = 0.5$) and for the different values of the anisotropy η . Figures (c)-(e) illustrate the detailed view for the respective cases (see the subcations).

$$-\sqrt{\frac{1 + \alpha_{n+1}}{\eta\beta_L}} + \mathcal{O}(\eta^{1/2}). \quad (19)$$

This means that we have very weakly interacting horizontal rows of junctions and the dispersion laws for them are strongly separated from each other. In the opposite limit $\eta \rightarrow \infty$ the junctions in the vertical subsystem are coupled much stronger as compared to the horizontal direction. Thus, there is very small difference between the oscillations within one vertical column of junctions. As a result, this can be viewed as each column oscillating as a whole, and, consequently the branches $\omega_{n>0}$ in figure 4b are very weakly separated and look almost identical.

Finally we discuss the behavior of the almost flat bands for the different values of anisotropy. This behavior is illustrated in figures 4c-4e. The total width of the almost flat band ($\omega_{n<0}$) is defined as a difference between the highest frequency value of the highest lying branch which is $\omega_{-1}(q)$ and the smallest value of the lowest branch

$$\Delta_- = \max_{q \in [-\pi, \pi]} \omega_{-1}(q) - \min_{q \in [-\pi, \pi]} \omega_{-N+1}(q) = \omega_{-1}(\pi) - (1 - \gamma^2)^{1/4}. \quad (20)$$

In the limit of small η or small β_L one can obtain the following asymptotic behavior of the plasmon frequency at the Brillouin zone edge:

$$\omega_{n<0}(\pi) = \begin{cases} \left[1 - \frac{1 - \sqrt{1 - \gamma^2}}{4\eta + 1 + \alpha_{n+1}} (1 + \alpha_{n+1}) \right]^{1/2}, & \beta_L \rightarrow 0, \\ (1 - \gamma^2)^{1/4}, & \eta \rightarrow 0. \end{cases} \quad (21)$$

The limit $\eta \rightarrow 0$ is illustrated in figure 4c. In this limit $\Delta_- \rightarrow 0$, hence, the whole band becomes flat. If we keep the anisotropy η constant and decrease the inductance the band width will depend on the number of rows, N , because $\alpha_2 = 1 - 2 \cos \pi/N$. As a result, Δ_- does not tend to 0.

In the limit of large β_L or η the limiting frequency value is given by

$$\omega_{n<0}(\pi) = \begin{cases} (1-\gamma^2)^{1/4}, & \beta_L \rightarrow \infty, \\ \left\{ \begin{array}{l} 1, \sqrt{1-\gamma^2} + \frac{4}{\beta_L} > 1 \\ \left[\sqrt{1-\gamma^2} + \frac{4}{\beta_L} \right]^{1/2}, \sqrt{1-\gamma^2} + \frac{4}{\beta_L} < 1 \end{array} \right\}, & \eta \rightarrow \infty. \end{cases} \quad (22)$$

In the limit when $\beta_L \rightarrow \infty$ for η fixed we again expect complete flattening of the $\omega_{n<0}$ band. The situation becomes more subtle if β_L is finite and $\eta \rightarrow \infty$. If discreteness is quite significant, or, alternatively, the bias is strong enough to guarantee the inequality $\beta_L > 4/(1 - \sqrt{1 - \gamma^2})$ one can obtain flattening when the strong discreteness limit is taken:

$$\Delta_- = \left[\sqrt{1-\gamma^2} + \frac{4}{\beta_L} \right]^{1/2} - (1-\gamma^2)^{1/4} \rightarrow_{\beta_L \rightarrow \infty} 0. \quad (23)$$

In the opposite case the band does not flatten because $\Delta_- = 1 - (1 - \gamma^2)^{1/4}$. This particular case is illustrated in figure 4e where the plasmon branches have relatively sharp minimum for $|q| < 1$ and flatten only when q approaches the Brillouin zone edge.

3.3. Spatial distribution of the Josephson phase vibrations

The respective eigenvectors $(\mathbf{A}^{(v)}, \mathbf{A}^{(h)}) = (A_1^{(v)}, \dots, A_{N-1}^{(v)}, A_1^{(h)}, \dots, A_N^{(h)})$ can be computed from the linear set of equations that emanates from the equations of motion (5)-(8). With the help of the matrices L , U and $D_{v,h}$ defined in Appendix A it is possible to write the equations for the eigenvectors in the following form:

$$[\omega_i^2(q) - \omega^2]A_n^{(v)} + \frac{1 - e^{-iq}}{\beta_L} (A_n^{(h)} - A_{n+1}^{(h)}) = 0, \quad n = \overline{1, N-1}, \quad (24)$$

$$(1 - e^{iq}) (A_n^{(v)} - A_{n-1}^{(v)}) - A_{n-1}^{(h)} - A_{n+1}^{(h)} + [2\beta_L\eta(1 - \omega^2) + 1]A_n^{(h)} = 0, \quad n = \overline{2, N-1}, \quad (25)$$

$$(1 - e^{iq})A_1^{(v)} + [\beta_L\eta(1 - \omega^2) + 1]A_1^{(h)} - A_2^{(h)} = 0, \quad (26)$$

$$(1 - e^{iq})A_N^{(v)} + A_{N-1}^{(h)} - [\beta_L\eta(1 - \omega^2) + 1]A_N^{(h)} = 0. \quad (27)$$

Long-wave limit $q = 0$. In this limit regardless of the particular eigenfrequency the plasmon modes of the vertical and horizontal sublattices decouple. As a result, the amplitudes of the vertical subsystem come as a solution of the strongly degenerate system of equations and are basically the eigenvectors of the diagonal matrix: $\mathbf{A}^{(v)} = [(1, 0, \dots, 0), (0, 1, \dots, 0), \dots, (0, 0, \dots, 1)]$. In the horizontal subsystem all the junctions are excited and their amplitudes satisfy more complex conditions as they are eigenvectors of the tridiagonal matrix. One of the eigenfrequencies coincides with the Josephson plasma frequency ($\omega_0 = 1$) and is dispersionless. The respective eigenvector consists of only horizontal junctions excited while all vertical ones are at rest as shown schematically in figure 5a. In the most degenerate case when the external bias is absent the general picture shown in figures 5a-5e does not change.

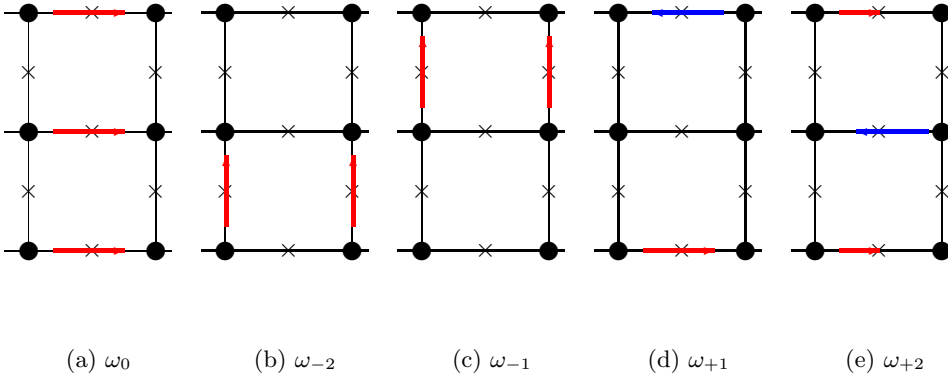


Figure 5: Schematic representation of the plasmon amplitude distribution for the array with $N = 3$ rows in the long wave limit $q = 0$. Color arrows correspond to the excited junctions where the red arrow (pointing right) and blue arrow (pointing left) represent positive (negative) amplitude of the respective junction. Arrows directed upwards describe excited vertical junctions. Unexcited junctions have no arrows. Subcaptions under each figure denote to which eigenvalue this eigenvector belongs.

Beyond the long-wave limit ($q \neq 0$). If one departs slightly from the center of the Brillouin zone ($q = 0$) the vibrations in the horizontal and vertical subsystems start to mix. For small values of dc bias the terms $\propto (1 - \cos q)$ start to appear in the components that were unexcited in the $q = 0$ limit. In the unbiased case there is $(N - 1)$ -fold degeneracy of the $\omega = 1$ eigenfrequency. The mode which initially was uniform with respect to horizontal vibrations and with no excited vertical vibrations now has both vertical and horizontal junctions excited. Similarly, the $\omega_0 = 1$ mode has also both vertical and horizontal junctions excited.

If the external bias γ is applied the degeneracy for the modes $\omega_{-N+1}, \dots, \omega_{-1}$ is lifted (except the central point $q = 0$). As a result, the $\omega_0 = 1$ mode retains the same structure as it had in the long-wave limit: $A_n^{(v)} = 0$, $n = \overline{1, N-1}$; $A_n^{(h)} = A \neq 0$, $n = \overline{1, N}$ (see also figure 5a). The modes that lie below the flat branch $\omega_n(q) < 1$, $n < 0$ have the same spatial structure as their counterparts above the flat branch. In other words, the spatial structure of ω_{-n} and ω_n modes will be the same for each n . The particular case for $N = 3$ is shown in figures 6a-6c. The modes with $\omega_{\neq 0}$ have certain symmetry with respect to the symmetry line that is parallel to the OX axis and cuts the array in halves. If the number of rows N is odd this line coincides with the $(N + 1)$ th row while if N is even this line lies in the middle between the $N/2$ th and $(N + 1)/2$ th rows. According to this symmetry, in the amplitude distribution of each mode either the vertical phases are excited in the antisymmetric way while the horizontal phases are excited in the symmetric way or vice versa. The figures 6b-6c clearly demonstrate that. At the edges of the Brillouin zone ($q = \pm\pi$) the structure of the non-flat bands becomes more symmetric with all the amplitudes of the horizontal junctions having the same absolute value.

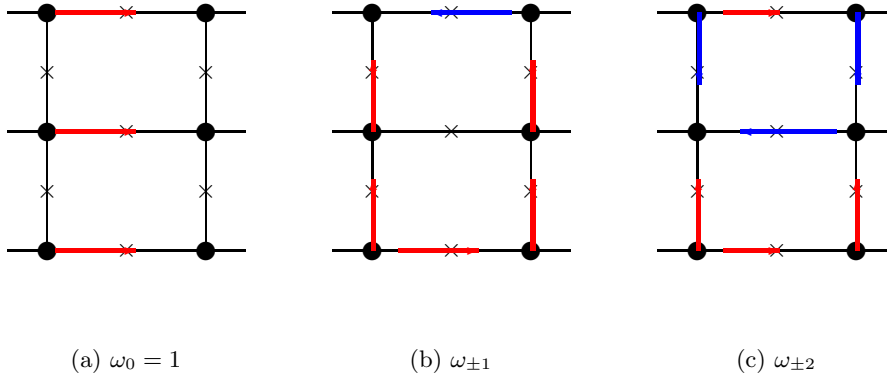


Figure 6: Schematic representation of the plasmon waves that correspond to different eigenfrequencies (see the respective subcaption) for $N = 3$ rows and $\gamma \neq 0$. The meaning of the color arrows is the same as in figures 5a-5e.

4. Discussion and conclusions

In this article the linear wave spectrum of the Q1D JJA is studied. The Q1D JJA is a multi-ladder array that is considered to be infinite in X direction and consists of N rows in Y direction. The array is uniformly biased by the dc current applied along the every vertical column. The main result can be summarized in the following way. The Josephson plasmon spectrum of the array consists of $2N - 1$ branches. In the unbiased case N branches are completely flat and the respective eigenfrequency coincides with the Josephson plasma frequency. The remaining $N - 1$ branches are strongly dispersive and their dispersion laws are similar to the standard 1D JJA dispersion relations. When the dc bias is applied the N -fold degeneracy is lifted and only one flat branch remains. This flat branch corresponds to the plasmon mode where all vertical junctions are not excited and all horizontal junctions oscillate in phase. The rest of the branches become weakly dispersive if the dc bias is small: $\gamma = I_B/I_c^{(v)} \ll 1$. In that case the width of all flat bands is confined by the limits $(1 - \gamma^2)^{1/4} \leq \omega < 1$.

The obtained Q1D JJA spectra are important for the studies of discrete breathers in these structures. While the discrete breather properties in the simple JJ ladder are well understood, their counterparts in more complex ladder-like structures have not been studied yet. The current studies of the linear spectra are the necessary first step in that direction. In particular, we would like to point out that in the limit of small horizontal-vertical anisotropy $\eta \ll 1$ there are large gaps between the plasmon modes. This opens a possibility of the gap discrete breathers [28] appearing in different gaps of the linear spectrum. Finally, the phenomenon of Fano resonances in the simplest JJ ladder [29] can be investigated for more complex Q1D JJAs.

Acknowledgments

Both the authors acknowledge the support by the National Research Foundation of Ukraine grant (2020.02/0051) "Topological phases of matter and excitations in Dirac materials, Josephson junctions and magnets".

Appendix A. Computation of the characteristic polynomial

This Appendix is devoted to the details of the characteristic polynomial computation. The characteristic polynomial is given by the determinant of the $2N - 1 \times 2N - 1$ matrix

$$\chi(\omega^2) = \det(A - \mathbb{I}_{2N-1}\omega^2), \quad A = \left[\begin{array}{c|c} D_v & U \\ \hline L & D_h \end{array} \right]. \quad (\text{A.1})$$

Here $D_v = \omega_i^2(q)\mathbb{I}_{N-1}$, \mathbb{I}_N is the $N \times N$ identity matrix, U is $N \times N - 1$ matrix, L is $N - 1 \times N$ matrix and D_h is tridiagonal $N - 1 \times N - 1$. These three matrices are given by the following expressions:

$$D_h \equiv \begin{bmatrix} 1+b & -b & 0 & \cdots & 0 & 0 & 0 \\ -b & 1+2b & -b & \cdots & 0 & 0 & 0 \\ 0 & -b & 1+2b & \cdots & 0 & 0 & 0 \\ \vdots & \vdots & \vdots & \ddots & \vdots & \vdots & \vdots \\ 0 & 0 & 0 & \cdots & -b & 1+2b & -b \\ 0 & 0 & 0 & \cdots & 0 & -b & 1+b \end{bmatrix}, \quad (\text{A.2})$$

$$U \equiv \frac{1 - e^{-iq}}{\beta_L} S, \quad S = \begin{bmatrix} 1 & -1 & 0 & \cdots & 0 & 0 & 0 \\ 0 & 1 & -1 & \cdots & 0 & 0 & 0 \\ 0 & 0 & 1 & \cdots & 0 & 0 & 0 \\ \vdots & \vdots & \vdots & \ddots & \vdots & \vdots & \vdots \\ 0 & 0 & 0 & \cdots & 1 & -1 & 0 \\ 0 & 0 & 0 & \cdots & 0 & 1 & -1 \end{bmatrix}, \quad (\text{A.3})$$

$$L \equiv \frac{1 - e^{iq}}{\beta_L \eta} S^T, \quad b \equiv \frac{1}{\beta_L \eta}. \quad (\text{A.4})$$

The term $\omega_i(q)$ is the dispersion law of the one-dimensional array of the biased vertical Josephson junctions (see [25, 27])

$$\omega_i^2(q) \equiv \sqrt{1 - \gamma^2} + \frac{2}{\beta_L}(1 - \cos q). \quad (\text{A.5})$$

With the help of Schur complement [30] it is possible to simplify the determinant of the matrix $A - \mathbb{I}_{2N-1}\omega^2$ [see equation (A.1)]:

$$\begin{aligned} \chi(\omega^2) &= \det(D_v - \omega^2\mathbb{I}_{N-1}) \det[D_h - \omega^2\mathbb{I}_N - L(D_v - \omega^2\mathbb{I}_{N-1})^{-1}U] = \\ &= [\omega_i^2(q) - \omega^2]^{N-1} \det \left[D_h - \omega^2\mathbb{I}_N - \frac{1}{(\omega_i^2(q) - \omega^2)} LU \right], \end{aligned} \quad (\text{A.6})$$

$$LU = \frac{|1 - e^{iq}|^2}{\eta\beta_L^2} \begin{bmatrix} 1 & -1 & 0 & \cdots & 0 & 0 & 0 \\ -1 & 2 & -1 & \cdots & 0 & 0 & 0 \\ 0 & -1 & 2 & \cdots & 0 & 0 & 0 \\ \vdots & \vdots & \vdots & \ddots & \vdots & \vdots & \vdots \\ 0 & 0 & 0 & \cdots & -1 & 2 & -1 \\ 0 & 0 & 0 & \cdots & 0 & -1 & 1 \end{bmatrix}. \quad (\text{A.7})$$

The matrix in $[\cdots]$ is an $N \times N$ tridiagonal matrix. The resulting characteristic polynomial can be written as a determinant of the tridiagonal matrix D_N :

$$\chi(\omega^2) = \frac{\det D_N}{\eta^N [\omega_i(q) - \omega]}, \quad (\text{A.8})$$

$$D_2 = \begin{bmatrix} d_0 & d_1 \\ d_1 & d_0 \end{bmatrix}, \quad D_N = \begin{bmatrix} d_0 & d_1 & 0 & \cdots & 0 & 0 & 0 \\ d_1 & d_2 & d_1 & \cdots & 0 & 0 & 0 \\ 0 & d_1 & d_2 & \cdots & 0 & 0 & 0 \\ \vdots & \vdots & \vdots & \ddots & \vdots & \vdots & \vdots \\ 0 & 0 & 0 & \cdots & d_2 & d_1 & 0 \\ 0 & 0 & 0 & \cdots & d_1 & d_2 & d_1 \\ 0 & 0 & 0 & \cdots & 0 & d_1 & d_0 \end{bmatrix}, \quad (\text{A.9})$$

with

$$d_0 = \eta[\omega_i^2(q) - \omega^2] \left(1 + \frac{1}{\eta\beta_L} - \omega^2 \right) - \frac{2(1 - \cos q)}{\beta_L^2}, \quad (\text{A.10})$$

$$d_1 = -\frac{1}{\beta_L}[\omega_i^2(q) - \omega^2] + \frac{2(1 - \cos q)}{\beta_L^2}, \quad (\text{A.11})$$

$$d_2 = d_0 - d_1 = \eta[\omega_i^2(q) - \omega^2] \left(1 + \frac{2}{\eta\beta_L} - \omega^2 \right) - \frac{4(1 - \cos q)}{\beta_L^2}, \quad (\text{A.12})$$

Note that the matrix D_2 does not contain the d_2 element

In general, the determinant $\det D_N$ can be factorized if the matrix D_N can be diagonalized. The eigenvalues of this tridiagonal matrix are known [31]:

$$\lambda_n = d_0 + \left[-1 + 2 \cos \frac{\pi(n-1)}{N} \right] d_1, \quad n = \overline{1, N}. \quad (\text{A.13})$$

Therefore, the determinant of the matrix D_N can be written explicitly. Also it should be taken into account that there always exists the first eigenvalue, $\lambda_1 = d_0 + d_1$. This will help to remove the singular term in the characteristic polynomial.

$$\begin{aligned} \det D_N &= \prod_{n=1}^N \left\{ d_0 + \left[-1 + \cos \frac{\pi(n-1)}{N} \right] d_1 \right\} = (d_0 + d_1) \times \\ &\times \prod_{n=2}^N \left\{ d_0 + \left[-1 + \cos \frac{\pi(n-1)}{N} \right] d_1 \right\}. \end{aligned} \quad (\text{A.14})$$

As a result, the characteristic polynomial for the squared frequency can be written as a product:

$$\chi(\omega^2) \propto (\omega^2 - 1) \prod_{n=2}^N [d_0 - \alpha_n d_1], \quad \alpha_n = 1 - 2 \cos \frac{\pi(n-1)}{N}. \quad (\text{A.15})$$

The roots of this polynomial are given by the equation $\omega^2 = 1$ and equation $d_0 = \alpha_n d_1$. Note that d_0 and d_1 are polynomials for ω^2 given by equations (A.10)-(A.11). Equation $d_0 = \alpha_n d_1$ transforms (the subscript n has been dropped for the sake of simplicity) into the quadratic equation for ω^2 :

$$\omega^4 - \left(1 + \omega_i^2 + \frac{1 + \alpha}{\eta\beta_L}\right) \omega^2 + \omega_i^2 \left(1 + \frac{1 + \alpha}{\eta\beta_L}\right) - 2(1 + \alpha) \frac{1 - \cos q}{\eta\beta_L^2} = 0. \quad (\text{A.16})$$

The roots of the abovementioned equation are

$$\omega^2(q) = \frac{1}{2} \left(1 + \omega_i^2 + \frac{1 + \alpha}{\eta\beta_L}\right) \pm \sqrt{\frac{1}{4} \left[\omega_i^2 - \left(1 + \frac{1 + \alpha}{\eta\beta_L}\right)\right]^2 + 2(1 + \alpha) \frac{1 - \cos q}{\eta\beta_L^2}}. \quad (\text{A.17})$$

ORCID iDs

Daryna Bukatova <https://orcid.org/0000-0002-0522-851X>

Yaroslav Zolotaryuk <https://orcid.org/0000-0003-1079-0221>

References

- [1] S. Flach D. Leykam, A. Andreanov. Artificial flat band systems: from lattice models to experiments. *Adv. in Phys.*, 3:1473052, 2018.
- [2] Bill Sutherland. Localization of electronic wave functions due to local topology. *Phys. Rev. B*, 34:5208–5211, Oct 1986.
- [3] Elliott H. Lieb. Two theorems on the hubbard model. *Phys. Rev. Lett.*, 62:1201–1204, Mar 1989.
- [4] Oleg Derzhko, Andreas Honecker, and Johannes Richter. Low-temperature thermodynamics for a flat-band ferromagnet: Rigorous versus numerical results. *Phys. Rev. B*, 76:220402, Dec 2007.
- [5] I. M. Pop, K. Hasselbach, O. Buisson, W. Guichard, B. Pannetier, and I. Protopopov. Measurement of the current-phase relation in josephson junction rhombi chains. *Phys. Rev. B*, 78:104504, Sep 2008.
- [6] A. Andreanov and M.V. Fistul. Resonant frequencies and spatial correlations in frustrated arrays of josephson type nonlinear oscillators. *J. Phys. A: Math. Theor.*, 52:105101, 2019.
- [7] T.T. Heikkilä and G.E. Volovik. Dimensional crossover in topological matter: Evolution of the multiple dirac point in the layered system to the flat band on the surface. *Jetp Lett.*, 93:59–65, 2011.
- [8] E. V. Gorbar, V. P. Gusynin, and D. O. Oriekhov. Gap generation and flat band catalysis in dice model with local interaction. *Phys. Rev. B*, 103:155155, Apr 2021.
- [9] Rodrigo A. Vicencio, Camilo Cantillano, Luis Morales-Inostroza, Bastián Real, Cristian Mejía-Cortés, Steffen Weimann, Alexander Szameit, and Mario I. Molina. Observation of localized states in lieb photonic lattices. *Phys. Rev. Lett.*, 114:245503, Jun 2015.
- [10] Shintaro Taie, Hideki Ozawa, Tomohiro Ichinose, Takuei Nishio, Shuta Nakajima, and Yoshiro Takahashi. Coherent driving and freezing of bosonic matter wave in an optical lieb lattice. *Science Advances*, 1(10), 2015.
- [11] D. V. Averin, K. Rabenstein, and V. K. Semenov. Rapid ballistic readout for flux qubits. *Phys. Rev. B*, 73:094504, Mar 2006.
- [12] K. G. Fedorov, A. V. Shcherbakova, M. J. Wolf, D. Beckmann, and A. V. Ustinov. Fluxon readout of a superconducting qubit. *Phys. Rev. Lett.*, 112:160502, 2014.
- [13] M V Bastrakova, N V Klenov, V I Ruzhickiy, and A M Satanin. Propagation of short current pulses in josephson transition line and ultrafast qubit control. *Journal of Physics: Conference Series*, 1410(1):012142, dec 2019.

- [14] Wenbin Yu, K. H. Lee, and D. Stroud. Vortex motion in josephson-junction arrays near $f=0$ and $f=1/2$. *Phys. Rev. B*, 47:5906–5914, Mar 1993.
- [15] S. G. Lachenmann, T. Doderer, D. Hoffmann, R. P. Huebener, P. A. A. Booi, and S. P. Benz. Observation of vortex dynamics in two-dimensional josephson-junction arrays. *Phys. Rev. B*, 50:3158–3164, Aug 1994.
- [16] D. Abraimov, P. Caputo, G. Filatrella, M. V. Fistul, G. Yu. Logvenov, and A. V. Ustinov. Broken symmetry of row switching in 2d josephson junction arrays. *Phys. Rev. Lett.*, 83:5354–5357, Dec 1999.
- [17] L. M. Floria, J. L. Marín, P. J. Martinez, F. Falo, and S. Aubry. Intrinsic localization in the dynamics of a josephson-junction ladder. *Europhys. Lett.*, 36:539, 1996.
- [18] E. Trías, J. J. Mazo, and T. P. Orlando. Discrete breathers in nonlinear lattices: Experimental detection in a josephson array. *Phys. Rev. Lett.*, 84(4):741–744, 2000.
- [19] P. Binder, D. Abraimov, A. V. Ustinov, S. Flach, and Y. Zolotaryuk. Observation of breathers in josephson ladders. *Phys. Rev. Lett.*, 84(4):745–748, 2000.
- [20] P. Binder, D. Abraimov, and A. V. Ustinov. Diversity of discrete breathers observed in a josephson ladder. *Phys. Rev. E*, 62(2):2858–2862, Aug 2000.
- [21] S. Flach and C. R. Willis. Discrete breathers. *Phys. Rep.*, 295(5):182, 1998.
- [22] A. E. Miroshnichenko, S. Flach, M. V. Fistul, Y. Zolotaryuk, and J. B. Page. Breathers in josephson junction ladders: Resonances and electromagnetic wave spectroscopy. *Phys. Rev. E*, 64(6):066601, 2001.
- [23] K. K. Likharev. *Dynamics of Josephson Junctions and Circuits*. Gordon and Breach, New York, 1986.
- [24] M. Barahona and S. Watanabe. Row-switched states in two-dimensional underdamped josephson-junction arrays. *Physical Review B*, 57, 5 1998.
- [25] A. V. Ustinov. Solitons in josephson junctions. *Physica D*, 123(1-4):315–329, 1998.
- [26] A. V. Ustinov, M. Cirillo, and B. A. Malomed. Fluxon dynamics in one-dimensional josephson-junction arrays. *Phys. Rev. B*, 47:8357–8360, 1993.
- [27] S. Watanabe, S. H. Strogatz, H. S. J. van der Zant, and T. P. Orlando. Whirling modes and parametric instabilities in the discrete sine-gordon equation: experimental tests in josephson rings. *Phys. Rev. Lett.*, 74:23, 1995.
- [28] Yuri S. Kivshar and Nikos Flytzanis. Gap solitons in diatomic lattices. *Phys. Rev. A*, 46:7972–7978, Dec 1992.
- [29] A. E. Miroshnichenko, M. Schuster, S. Flach, M. V. Fistul, and A. V. Ustinov. Resonant plasmon scattering by discrete breathers in josephson junction ladders. *Phys. Rev. B*, 71:174306, May 2005.
- [30] Fuzhen Zhang. *The Schur Complement and Its Applications*. Numerical Methods and Algorithms. Springer, Boston, MA, 2005.
- [31] Wen-Chyuan Yueh. Eigenvalues of several tridiagonal matrices. *Applied Mathematics E-Notes [electronic only]*, 5:66–74, 2005.